Research Article

Cheng Hu#, Lina Wu#, Changchun Zhou*, Huan Sun, Peng Gao, Xiujuan Xu, Chenxi Zhang, Jie Liang, Yujiang Fan, Jianxun Sun*, Xuedong Zhou, and Xingdong Zhang

Berberine/Ag nanoparticle embedded biomimetic calcium phosphate scaffolds for enhancing antibacterial function

https://doi.org/10.1515/ntrev-2020-0046
received April 23, 2020; accepted May 27, 2020

Abstract: In the past decade, biomimetic calcium phosphate (CaP) ceramics have been considered as practicable grafts and biomaterial substitutes in repairing jaw bone defect after tumor resection or traffic accident. Nowadays, increasing incidence of biomedical material-associated infection has raised a concern when applying these materials. In this work, a new porous CaP scaffold with antibacterial coating was proposed. This biomimetic scaffold was composited with berberine (BBR), Ag nanoparticles (nAg), and silk fibroin (SF). The microstructures and phase composition of the scaffolds were analyzed. The cytocompatibility and osteogenic potential of the prepared samples were evaluated *in vitro*. The scaffolds held hierarchical structure: the first-level porous CaP ceramic with micron pores ranged from 250 to 600 μm; the second-level spongy-like structure with abundant capillary pores ranged from 500 nm to 10 μm; and the third-level structure was achieved by filling BBR, nAg, and SF gel coatings into the above porous structures. The experimental results showed that the antimicrobial capability of single BBR coating is inconspicuous. However, the introduction of nAg could significantly promote the antibacterial effect of scaffolds. At the same time, such scaffolds showed improved osteoinductivity. This new biomimetic CaP scaffold with antibacterial and osteoinductive properties may be a promising candidate for bone tissue engineering.

Keywords: calcium phosphate bioceramic, biomimetic scaffold, hierarchical porosity, osteogenesis, antibacterial function

1 Introduction

Biomimetic design, structures, and biological functions of biomaterials are very important for promoting scaffold repair or regenerating tissues [1–3]. Due to good biocompatibility, biological activity, and absorbable degradation, calcium phosphate (CaP) biomaterials have been extensively used as autologous bone graft substitute [4]. Nevertheless, various potential infections associated with CaP bone implants may cause delayed union, implant failure, and even life threatening. Hence, it is necessary to apply empiric antibiotic therapy or prophylactic use of antibiotics to prevent the infection [4,5]. While large doses of antibiotics applied clinically may induce the appearance of drug-resistance strains and decrease the drug efficiency [6]. To address this problem, introducing local sustained-release antimicrobial coatings without antibiotic might be a practicable surface modification method.

Recent research studies indicate that certain traditional Chinese medicine (TCM) have an inhibitory activity on bacteria and some might even reverse bacterial resistance [7,8]. *Coptidis rhizoma* is one of the most frequently used herbs prescribed for treating bacterial gastroenteritis. The effective component of this herb is berberine (BBR), an isoquinoline alkaloid. BBR has been reported to have effective antimicrobial activity against

# These authors contributed equally to this paper.

* **Corresponding author: Changchun Zhou,** National Engineering Research Center for Biomaterials, Sichuan University, 610064, Chengdu, China, e-mail: changchunzhou@scu.edu.cn
* **Corresponding author: Jianxun Sun,** State Key Laboratory of Oral Diseases, West China Hospital of Stomatology, Sichuan University, Chengdu 610041, China, e-mail: jxsun@scu.edu.cn
Cheng Hu, Peng Gao, Chenxi Zhang, Xuedong Zhou: State Key Laboratory of Oral Diseases, West China Hospital of Stomatology, Sichuan University, Chengdu 610041, China
Lina Wu, Huan Sun, Xiujuan Xu, Jie Liang, Yujiang Fan, Xingdong Zhang: National Engineering Research Center for Biomaterials, Sichuan University, 610064, Chengdu, China

bacteria, fungi, protozoans, and viruses, especially when applied to fight against Gram-positive bacteria [9,10]. Moreover, BBR was demonstrated to have a good antibacterial activity against multidrug resistant *Escherichia coli* [11] and to be an enhancer of the activity of azithromycin when treating methicillin-resistant *Staphylococcus aureus* (MRSA) infections [12]. Chu et al. [13] found that the formation of MRSA's amyloid fibrils, which consist of phenol-soluble modulins (PSMs), could be suppressed by BBR, and further study demonstrated that BBR could inhibit the aggregation of PSMs into amyloid fibrils through binding to Phe19 in PSMα2. Actually, it exhibited evident bacteriostatic action at relative low concentration and germicidal action at high concentration [14]. Besides, BBR could enhance the osteogenic differentiation of human bone marrow-derived mesenchymal stem cells by promoting Runx2 expression and activating canonical Wnt/β-catenin signaling pathway [15].

Although the antibacterial effect of BBR has been proven, the efficacy of this drug is limited by its concentration. To enhance the antibacterial performance, the compound application of other ingredients is needed. Silver-composited biomaterials have attracted much attention in enhancing the antibacterial properties of implants due to their stable character and powerful germicidal efficacy [16,17]. Ag nanoparticles (nAg) show much higher antibacterial activity than common silver products, which may be because of their nanoscale size, large surface area, and high surface activity [18,19]. When come into contact with fluids, nAg can react with water to form Ag ions. Simultaneously, with nanoscale size and ions, nAg can easily get access to the inside of pathogen, then directly inactivate metabolic enzymes and damage DNA [20–22].

In our work, a BBR/nAg/silk fibroin (SF) functional layer was built on the CaP substrate. The porous CaP ceramic had various pores, providing more interfaces for coating attachment. SF is a widely used material in tissue engineering [23,24]. The structure of SF is similar to that of Col I, which can help to manufacture a microenvironment like the natural structure [25]. A recent study reported that under light, SF could offer a homogeneous atmosphere and reduce chemical groups, so that nAg could be produced *in situ* [26]. Furthermore, SF could transfer its conformation into β-sheet when exposed to high temperature or some organic solvent, for better cytocompatibility and mechanical properties [27].

In this paper, antibiotic-free BBR/nAg/SF-composited biomimetic CaP scaffolds were developed to enhance the antibacterial and osteogenesis activity. The functional designs of CaP scaffold coated with SF, BBR/SF, and BBR/nAg/SF were marked as CPS, CPSB, and CPSBA specimens, respectively. The CaP was produced through the gas foaming method. For further modifications, the SF was applied. The link between coating and CaP substrates was polydopamine (PDA) layer. Then, the mixed SF solution was dropped on the CaP substrates. For CPSBA group, the origin BBR/nAg/SF mixture had experienced the UV explosion to reduce silver ions *in situ*. The cytocompatibility, antimicrobial activity, and osteoinductivity were evaluated *in vitro*. This new biomimetic CaP scaffold with functionalized coating would be expected to show satisfying antibacterial capabilities *in vitro* and exhibit acceptable biocompatibility and osteoinductive activities.

2 Materials and methods

2.1 Preparation of multilevel biomimetic CaP scaffolds

The fabrication of the multilevel biomimetic CaP scaffolds is shown in Figure 1. The precursor CaP powders (hydroxyapatite/β-tricalcium phosphate = 30:70; National Engineering Research Center for Biomaterials, Chengdu, China) were synthesized by the wet chemical method according to the following procedure. Five liters of 0.85 mol/L $Ca(NO_3)_2$ (Aladdin, Shanghai) solution was dropped slowly into 5 mL of 0.55 mol/L $(NH_4)_2HPO_4$ (Aladdin, Shanghai) solution under stirring at room temperature. The pH of this solution was maintained at 8 by the addition of ammonium hydroxide (Aladdin, Shanghai) solution. The reaction solution was stirred for 6 h and aged for 24 h. The reaction precipitate was then collected, washed with deionized water, dried, and crushed into powder with a particle size of about 50–100 μm. The first-level porous structures of the CaP ceramics were produced by using the H_2O_2 foaming method. Approximately 200 g of CaP powder, 15 mL of polyvinyl alcohol (Aladdin, Shanghai), 15 mL of cellulose, 50 mL of H_2O_2 (Aladdin, Shanghai), and 120 mL of deionized water were mixed to form a ceramic slurry. This slurry was heated for 2 min in a microwave to generate gas and then molded in a wooden mold to obtain the porous ceramic green body. Afterward, the second-level microscale porous CaP ceramics were obtained via a two-step sintering strategy. The green body was dried at 80°C for 12 h and then heated (heating rate: 10°C/min) to a high temperature ($T1$ = 1100°C, hold

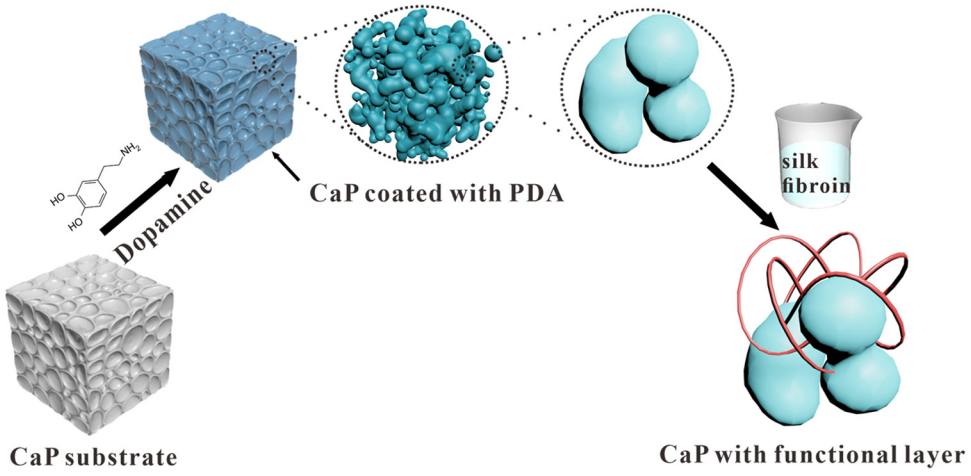

Figure 1: Schematic of fabrication process of BBR/nAg/SF multilevel biomimetic CaP scaffolds.

2 h) to achieve intermediate fusion. Subsequently, the samples were rapidly cooled down to *T*2 (*T*1 = 950°C, hold 2 h, cooling rate: 30°C/min) and maintained at this temperature for a certain amount of time. Finally, the samples were cooled to room temperature. The porosity of the prepared CaP ceramic was determined by the mercury intrusion method. The third-level BBR/nAg/SF layer was fabricated by perfuse coating.

2.2 Coating of multilevel BBR/nAg/SF layer

BBR powders (Bailingwei, Beijing) were first dissolved in dimethyl sulfoxide (Aladdin, Shanghai) to prepare a concentrated solution. Then, $AgNO_3$ (Haoyi, Chengdu) and BBR solution were added into a 2 wt% SF (Yuanye, Shanghai) solution to prepare the solution mixture. The final $AgNO_3$ and BBR concentrations in the solution were 0.2 mM/L and 0.60 mg/mL, respectively. Meanwhile, the concentration of dimethyl sulfoxide remained the same within the groups. Then, the SF/BBR/$AgNO_3$ solution was exposed in the atmosphere to a 100 W UV lamp (Kenggewang, Chengdu) at room temperature for 20 min *in situ* to form nAg. Then, the mixture composite solution was reserved at −20°C for the follow-up experiment. CaP scaffolds were immersed into 2 mg/mL dopamine hydrochloride prepared with Tris–HCl buffer (10 mM, pH = 8.5) for 24 h in darkness at 37°C; then, ultrasound cleaning was performed on all the scaffolds. The generated PDA (Aladdin, Shanghai) layer on the CaP scaffolds played an auxiliary role in bonding SF mixture coating. These functional coatings were obtained by a dipping–drying process. Finally, the samples were dried in an oven at 80°C for 30 min.

2.3 Microstructures and mechanical properties characterization

Microstructure of the prepared scaffolds was observed by a scanning electron microscope (SEM, JSM-7500F; JEOL, Tokyo, Japan). All the specimens were observed before dehydration and spray gold treatment. The elemental components of the surface were measured by energy-dispersive X-ray spectroscopy (EDS; Quanta 200).

The mechanical properties of the prepared samples were measured by dynamic mechanical analysis (Precision Universal Tester Autograph AG-X, Japan) at 20°C. The sample were cylinder shaped, with a thickness of 10 mm. Prior to the measurement, the dimensions of the samples were corrected by a digital micrometer. The properties were tested with a strain amplitude of 70 μm. The compressive modulus was obtained from dynamic compressive curves. The elastic region ranges from 2% to 6%. The parameters were determined according to the finite difference method [28].

2.4 *In vitro* BBR release and antibacterial performance test

To explore the release mode of BBR during *in vitro* degeneration, the CPSB samples were immersed in a 2 mL phosphate buffer saline solution. At one specific time point, the leaching solution was collected. Due to the linear relation between the absorbance and BBR concentration, the collected samples were measured with a spectrophotometer (Thermo Fisher, 1510, Finland), and the data were transferred to a concentration unit.

S. aureus (ATCC 29523) were cultured in a sterilized Luria–Bertani (LB) broth at 37°C for 24 h, and then,

400 μL of solution containing 10^6 CFU/mL of bacteria was dropped on each specimen (sterilized by ultra violet) in 48-well plates. Subsequently, the plates were incubated at 37°C for 24 h, then the specimens were taken out. After fixation with 2.5% (v/v) glutaraldehyde and dehydration (each dehydration step lasted for 10 min) in a series of ethanol concentration (35, 50, 75, 90, 95, and 100%), the morphologies of the anchored bacteria were investigated by SEM observations. Before SEM observation, the dried samples needed to be spluttered with gold particles to increase their electrical conductivity.

The bacterial inhibition zone was measured to evaluate the antimicrobial activity. One hundred microliters of solution containing 10^7 CFU/mL of bacteria was evenly sprayed on the surface of the LB solid medium. Then, the samples were put onto the surface of the solid medium. After incubating for 24 h at 37°C, the inhibition zones surrounding the samples were observed and recorded with a camera.

To explore the growth curve of *S. aureus*, one tablet, each of the CaP, CPS, CPSB, and CPSBA samples, was immersed into 490 μL of culture medium to obtain the extracts [29]. Meanwhile, 10 μL of the 10^7 CFU/mL bacterial suspension was added into each group. The growth curves were plotted according to an optical density value of 600 nm and monitored every 30 min.

2.5 Cell viability and osteoinductivity test

The pre-osteoblasts MC3T3-E1 were employed to evaluate the cell cytotoxicity *in vitro*. The cells were cultured in Dulbecco's Modified Eagle Medium (Gibco-BRL Life Technologies) with 10% fetal bovine serum (Gibco-BRL Life Technologies) and 1% penicillin/streptomycin in a humidified atmosphere of 5% CO_2 at 37°C. After reaching 80–90% confluence, the cells were trypsinized and collected and counted by a hemocytometer. The cells were diluted to 1×10^5 cells/mL and seeded on presterilized samples, and the medium was refreshed every other day.

For cytoskeleton investigation, the cells were fixed in 4% paraformaldehyde, permeabilized, and then stained with rhodamine-labeled phalloidin and 4′,6-diamidino-2-phenylindole. The images were captured with a confocal laser scanning microscope (Leica-TCS-SP5; Leica, Germany). For cell proliferation assessment, cell counting kit-8 (CCK-8) assays were performed. On days 1, 3, and 5, the cells on the samples were incubated with a medium containing 10% CCK-8 solution at 37°C for 2 h, and the absorbance was measured at 450 nm.

After cells had been transplanted for 5 days, the medium was replaced with a mineralization induction medium, containing 50 mg/L ascorbate, 10 mM β-glycerophosphate, and 0.1 μM dexamethasone. After the cells had been cultured and induced for 7 and 14 days, quantitation of alkaline phosphatase (ALP) activity test was performed. First, MC3T3 on the samples were lysed by 1% Triton X-100. Then, the lysates were measured by *p*-nitrophenyl phosphate/endogenous ALP enzymatic reaction, and the absorbance at 405 nm was recorded. At the same time, total protein was measured by using BCA kit for normalizing the interference from different numbers of cells.

2.6 Statistical analysis

All data were expressed as mean ± standard deviation. Statistical analysis, including one-way ANOVA and *t*-test, was conducted. The P values <0.05 mean statistically significant.

3 Results and discussion

3.1 Scaffolds microstructures and porosity

Figure 1 shows the illustrative diagram of the multilevel structure of CaP substrate with BBR/nAg co-embedded SF coating. The first-level porous CaP ceramic with micron pores was fabricated by the gas foaming method to mimic the natural bone architecture. Figures 2 and 4a show the microstructures of the prepared porous CaP scaffolds. The porosity of CaP scaffolds was 75 ± 8%, and the first-level macropores were random ball-like shape and ranged from 300 to 500 μm in size. Most pores were interconnected with each other. The second-level capillary microscale pores ranged from 500 nm to 10 μm were formed during the two-step sintering process. The second-level porous structure containing abundant capillary pores was formed during the sintering period. These two porous structures provided large contact surface. Simultaneously, the porous interface enhanced the initial bonding with the surrounding tissues when implanted. The third-level structure was achieved by filling BBR, nAg, and SF gel liquid into the above porous structures. The third-level structure was the coating of the multilevel BBR/nAg/SF layer.

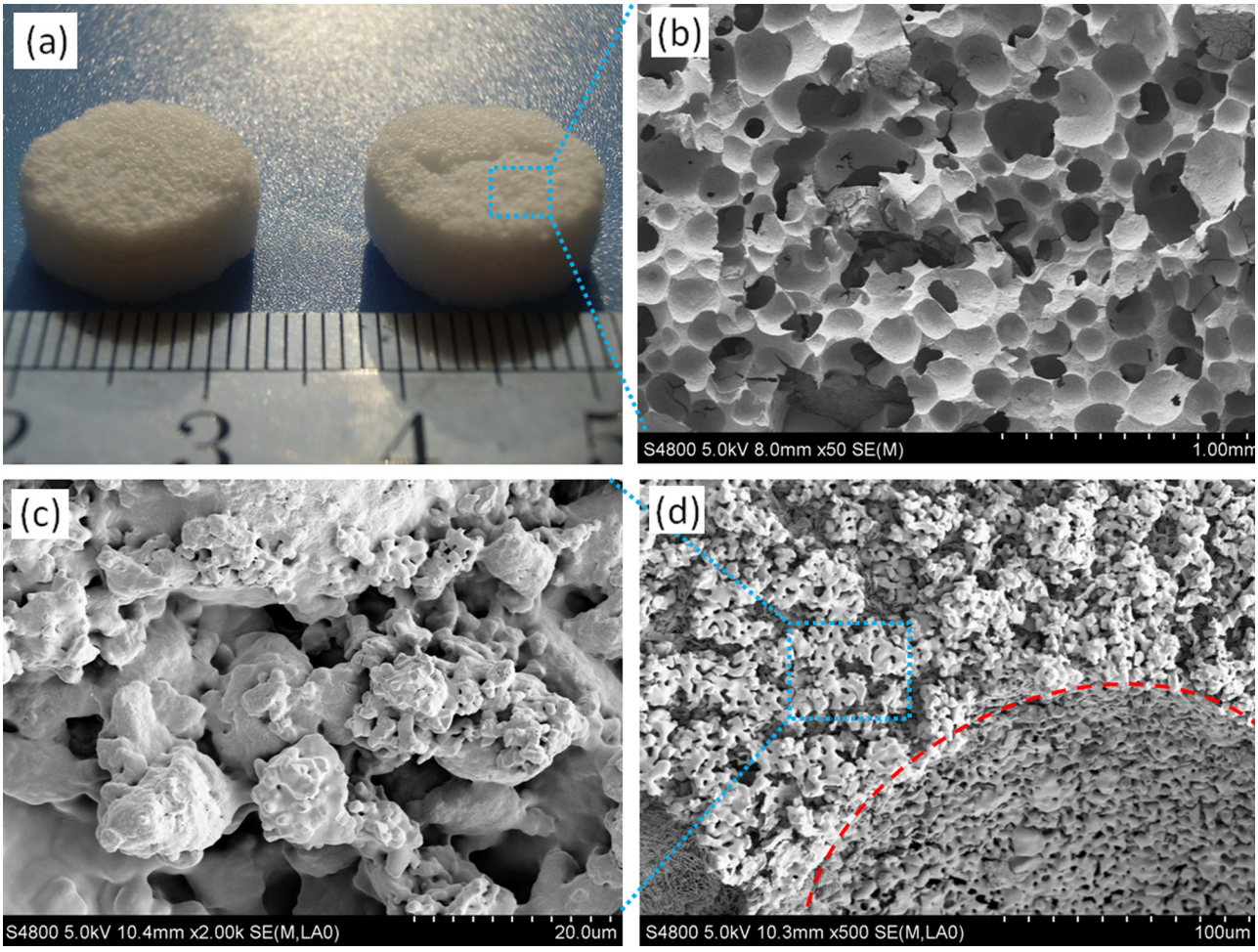

Figure 2: The microstructures of the porous CaP scaffolds. (a) The prepared porous CaP scaffolds were fabricated as round disc with a thickness of 3 mm and a diameter of 12 mm. (b) The first-level interconnected macropores were random ball-like shape and ranged from 300 to 500 μm. (c) Magnification of the second-level capillary micropores, which were ranged from 500 nm to 10 μm. (d) Second-level capillary micropores were formed during the two-step sintering process.

The synthesis mechanism of BBR/nAg/SF multi-biofunctional layer is shown in Figure 3. The CaP ceramic had various pores with size ranged from 250 to 600 μm. From a micro perspective, the varied CaP crystals fused with each other in the second-level porosity. For further modifications, the SF was applied. The link between BBR/nAg/SF coating and CaP substrates was provided by self-polymerization of PDA layer. The PDA layer makes it possible for thick SF layer to reach the deep side of the second-level structure. After the prepared mixed SF solution was instilled, all the samples were placed in a high-temperature environment to make SF coating change from random coil to β-conformation. For CPSBA group, the origin BBR/nAg/SF mixture had experienced the UV explosion to reduce silver ions *in situ*.

EDS elemental analysis (Figure 4b) verified that BBR and nAg had successfully loaded on CaP scaffolds through SF. The PDA layer and SF layer had provided nitrogen, chlorine, carbon, and sulfur. Nitrogen, chlorine, and carbon were also added into BBR. The nAg provided silver. The result indicated the BBR/nAg/SF coating had been successful prepared on CaP substrates.

PDA layer was used as a bridge to connect the BBR/nAg/SF layer to CaP bioceramics. Creating a PDA layer, as a common form of surface functionalized method, could increase hydrophilicity remarkably, making it possible for viscous fibroin to brim into the micropores of the second-level structure. On the other hand, the hydroxyl of PDA and the amine of fibroin reacted and combined. In short, the PDA provided a firm link for the third-level structure and simultaneously bioactivated the surface.

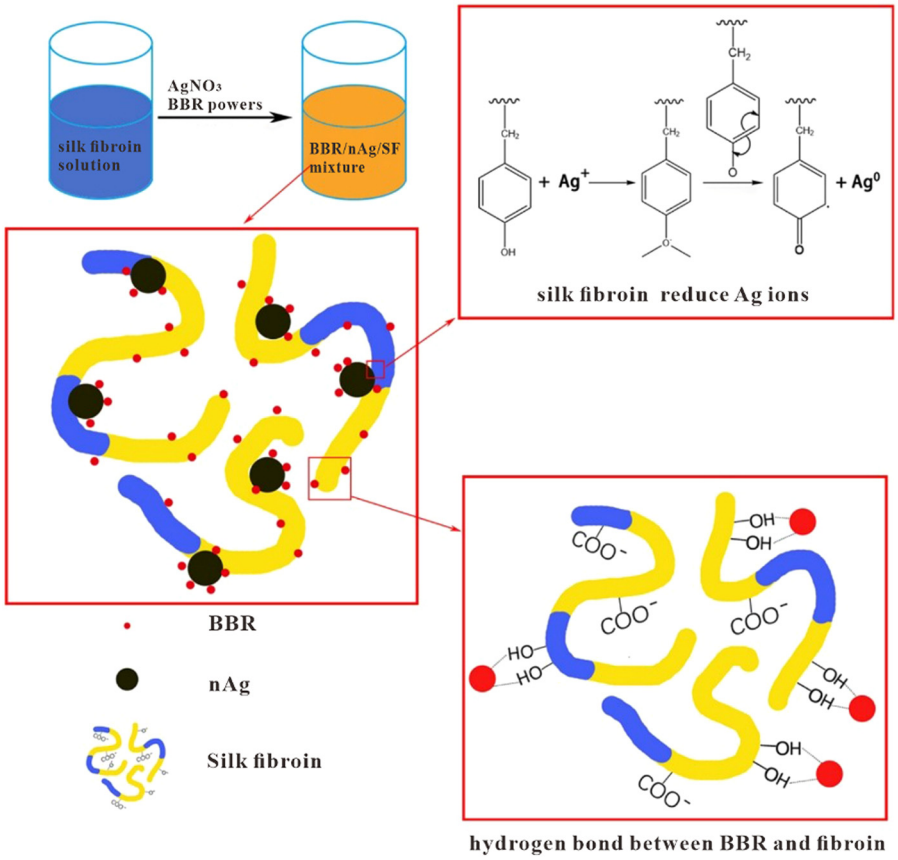

Figure 3: Synthesis mechanism of BBR/nAg/SF multi-biofunctional layer in CaP scaffolds.

Specific biofunctions may be enhanced by adding BBR and nAg into the biomimetic ceramic scaffolds. BBR is considered to be a promising addition to biomaterial due to its extensive and effective function similar to biological factor. Previous studies have demonstrated that bone tissue engineering scaffolds consisting of CaP can significantly improve the osteoinductivity [30]. At the same time, BBR has the similar effect against bone loss to icariin [31]. In our work, the natural bone tissue structure was simulated by using the CaP substrate (the porous structure similar to the skeleton) and SF coating (the fibroin coating similar to extracellular matrix [ECM]).

3.2 Mechanical properties characterization

Mechanical properties of previous scaffolds were explored (Table 1). CaP group exhibited an average maximum stress of 34.94 ± 9.33 N, indicating the brittleness of this material. The maximum stress of CPS group (SF/PDA layer fabricated CaP ceramics) reached to 55.39 ± 10.60 N, which is approximately 1.6 times higher than that of CaP. The promotion of CPS group was happened because the properties were enhanced after thick SF layer was formed. The maximum compressive strengths of the CaP and CPS groups were 1.46 ± 0.81 MPa and 2.74 ± 0.54 MPa, respectively. The result implied that this stable SF coating can reinforce the mechanical strength of CaP ceramic. The compressive modulus can reveal the resistance capability of the scaffolds under external force. The results also demonstrated that the compressive modulus of CPS group was enhanced compared with that of CaP, that is, from 104.00 ± 40.00 MPa to 181.00 ± 52.00 MPa (approximately 1.7 times). This mechanical characteristic is important for bone tissue applications.

3.3 Drug release properties and antibacterial function

In this study, antibiotic-free antimicrobial composite scaffolds were created, and the combination of BBR and nAg was proposed. The SF coating, which contained the abundant hydrophilic group such as hydroxyl group and

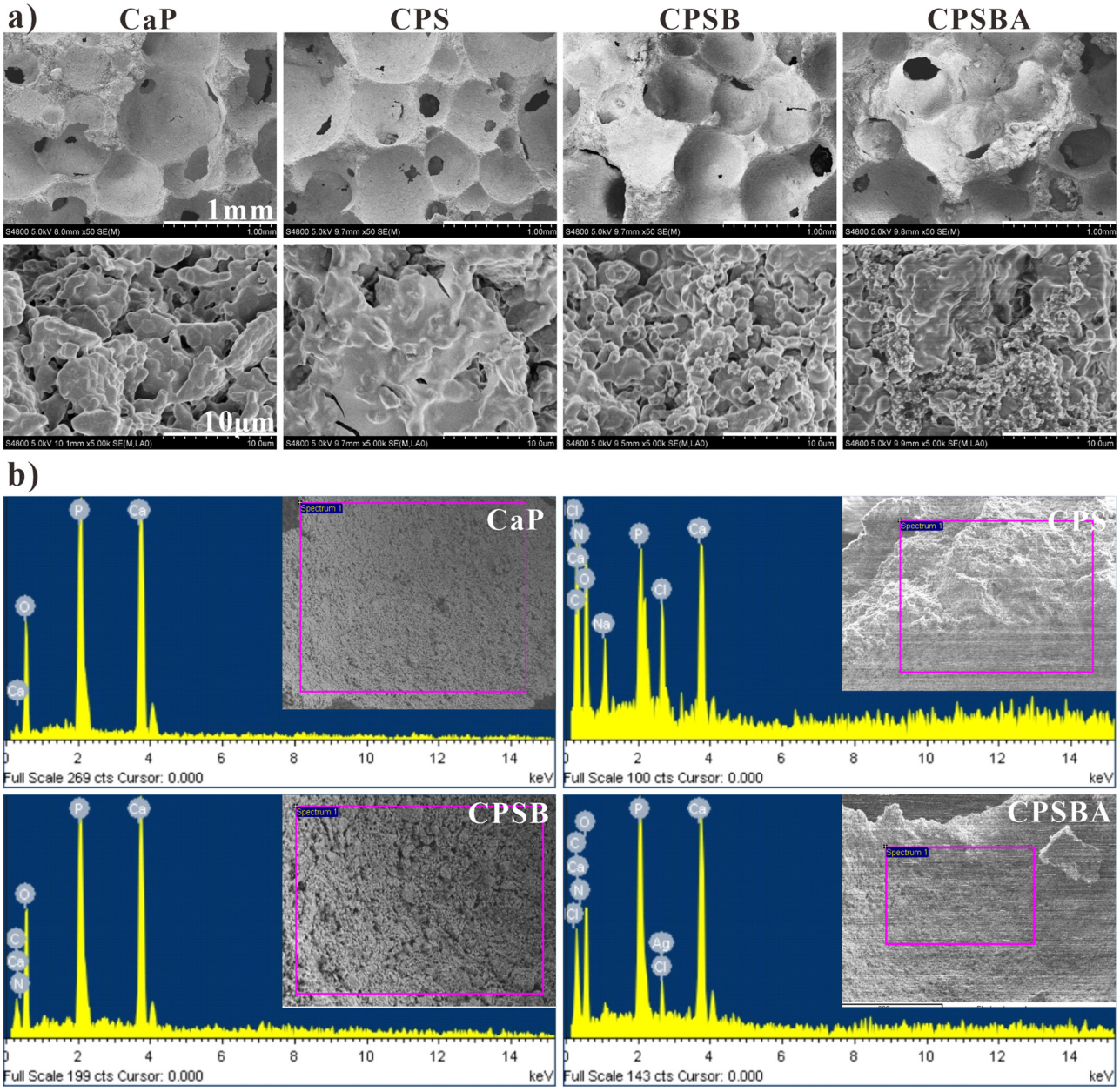

Figure 4: Surface characteristics. (a) Low- and high-magnification SEM images of calcium phosphate ceramic (CaP), CaP coated with SF (CPS), CaP coated with SF containing BBR (CPSB), and CaP coated with SF containing BBR and nAg (CPSBA). (b) EDS of CaP, CPS, CPSB, and CPSBA, demonstrating the successful deposition of SF, BBR, and nAg.

carboxyl group, integrated BBR molecule with hydrogen bonds. The *in vitro* BBR releasing examination showed that there was a stable controlled-release phenomenon (Figure 5d). The average total BBR was 17.85 μg per sample (n = 4). Drugs loaded on the scaffold were released rapidly in the early stages that prevents the hardness. The sustained-release trend of sample was in accordance with slightly soluble property of BBR and a previous study [32].

To further enhance the antimicrobial capability, nAg were used. As an extensive antibacterial agent, nAg has attracted a lot of attention. Recent studies have shown that fibroin can serve as a reducing agent to produce nAg. The SF molecules embody the 18 terminal amino acid residues, whose reducing capabilities are determined by the electron-donating ability of tyrosine (Tyr) [26]. When added to the green synthesis agent of nAg, the SF also stabilized these particles.

After cocultured with *S. aureus* for 1 day, the bacteria on scaffolds were fixed and observed with SEM. As shown in Figure 5a, bacteria adhered to and aggregated on the surface of bare CaP and SC groups. Their morphology stayed intact,

Table 1: Mechanical properties comparison of CaP and CPS specimens

Specimens	Average maximum stress (*N*)	Maximum compressive strength (MPa)	Compressive modulus (MPa)
CaP	34.94 ± 9.33	1.46 ± 0.81	104.00 ± 40.00
CPS	55.39 ± 10.60	2.74 ± 0.54	181.00 ± 52.00

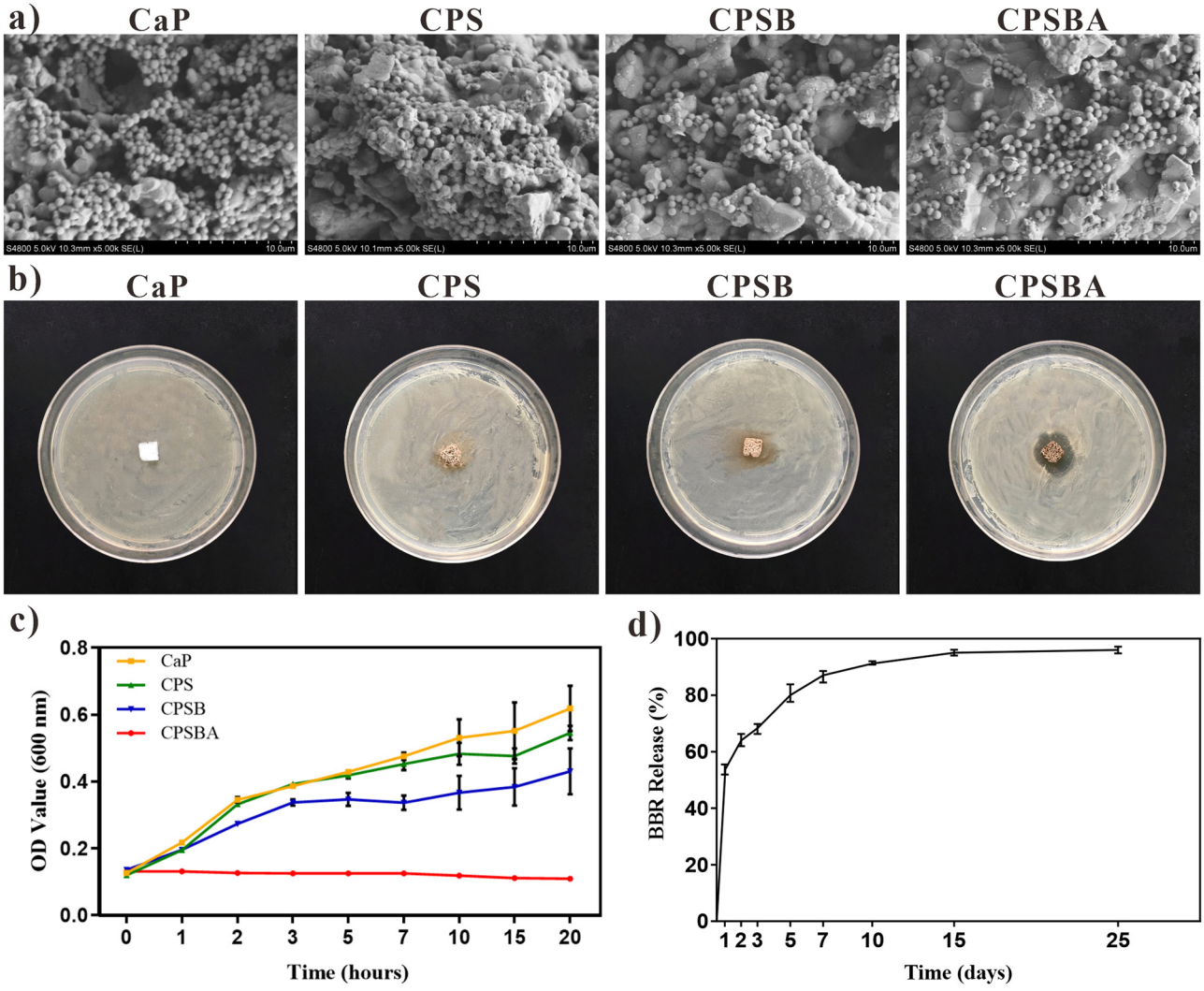

Figure 5: Antibacterial activities and BBR release curve. (a) Bacterial morphology, (b) bacterial inhibition ring test images of four groups of samples, (c) bacterial growth curve for incubating the extracts of CaP, CPS, CPSB, and CPSBA samples and *S. aureus* for 20 h, and (d) BBR release curve.

covering the surface of porous scaffolds. On the contrary, the bacteria immobilized by glutaraldehyde were few and scattered on the CPSB and CPSBA groups, with the debris of the bacteria being seen in the CPSBA group.

To further assess the efficiency of antimicrobial coating, bacterial inhibition ring test was performed. The CaP, CPS, and CPSB samples did not form obvious inhibition zone after incubating 24 h (Figure 5b), while the bacterial inhibition ring around the CPSBA sample displayed a vivid shape. Combined with the results of the bacterial growth curve (Figure 5c), it was found that the BBR coating may have certain bacteriostatic efficacy. The *S. aureus* growth curve in the CPSBA group had demonstrated that addition of nAg could greatly enhance the antimicrobial ability. The 24 h antibacterial rate of the CPSB and CPSBA groups was 36.23% and 98.23%, respectively.

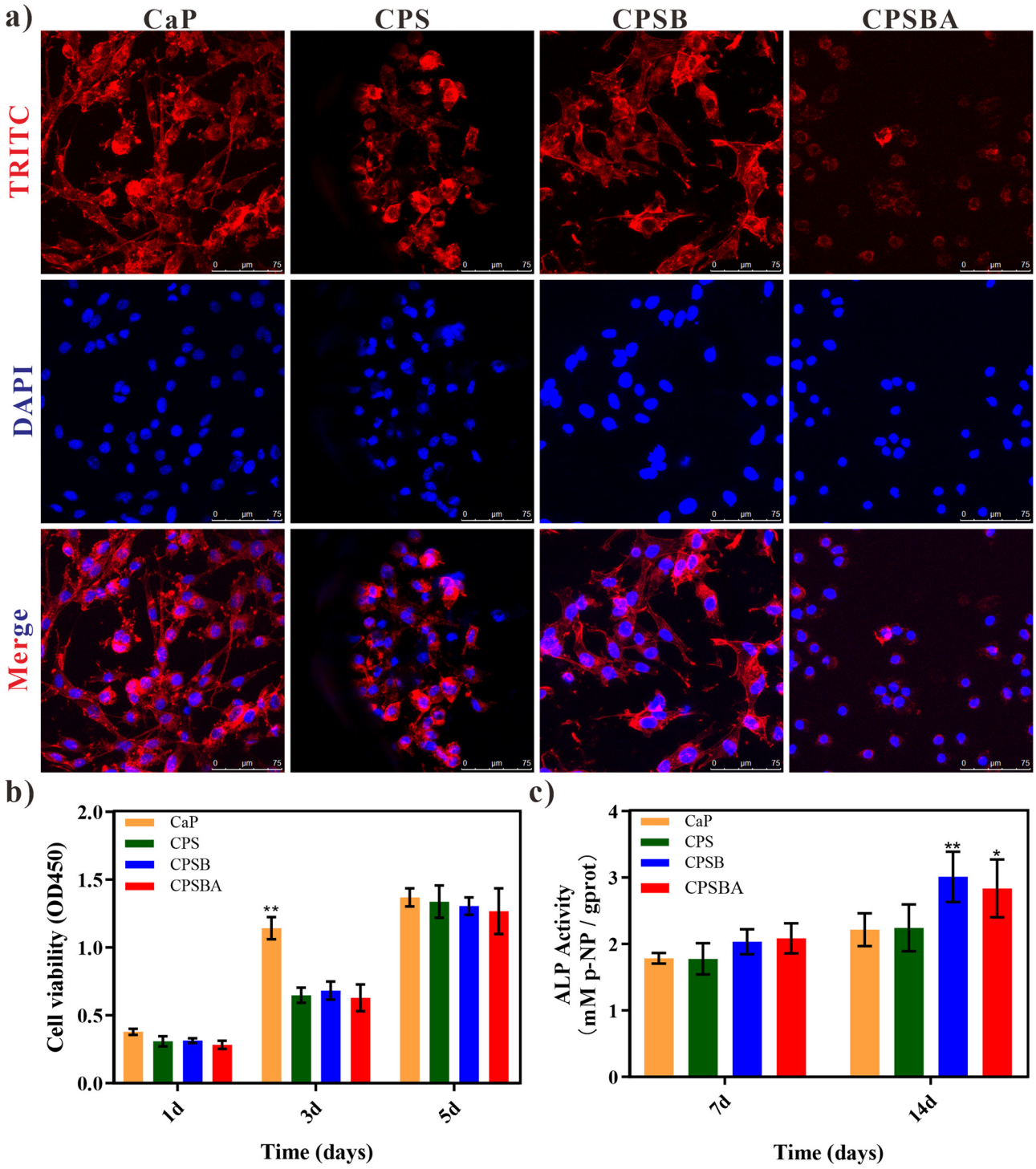

Figure 6: Cell viability. (a) Fluorescence staining of F-actin (red) and 4′,6-diamidino-2-phenylindole (blue) after culturing for 24 h; (b) cell proliferation via CCK-8 on days 1, 3, and 5; and (c) ALP activity of the MC3T3 cells incubated with CaP, CPS, CPSB, and CPSBA samples.

The antimicrobial capability of BBR is not strong. The bacterial adhesion results in the CPSB samples did not show the inaccessible images, because the porous surface morphology limited the scouring effect when the bacteria were fixed and dewatered on scaffolds. However, an apparent decrease in the bacterial density was observed, indicating that the local high BBR concentration had bacteriostatic efficacy. In another case, when put on the solid medium, the high content of BBR in surface coating could easily seep into a wide-range surrounding medium, as shown in the CPSB in Figure 5b (the yellow area around the samples). Thus, the concentration of BBR was

reduced, so that the inhibition ring was invisible. It is important to introduce nAg to promote the antibacterial effect of scaffolds. The final composite antibiotic-free coating exhibited extremely satisfactory germicidal efficacy. Simultaneously, the content of nAg was low, which had little impact on subsequent experiment.

3.4 Cell viability and osteoinductivity test

After incubating for 24 h, the cytoskeleton and nuclei were immunofluorescence stained to observe the spindle-like MC3T3-E1 (Figure 6a). Owing to the macropores, the cells were unevenly distributed. Cells that incubated on the surface of CaP and CPSB samples showed the stretching filament actin, while the other two groups were kind of stenotic. After loading BBR, cell morphology extended with the formation of pseudopodium on the CPSB samples. Nevertheless, the addition of nAg seemed to have increased the toxicity of MC3T3. Compared with CPSB group, the cells began to assemble and crimp. In semiquantitative analysis, the cell viability was assessed by CCK-8 kit (Figure 6b). There were similar results after 1- or 5-day incubation; however, variation in cell growth was shown after 3 days of culture. Cells on bare CaP scaffolds grown/adhered much better than those of other groups.

In vitro osteogenesis was evaluated (Figure 6c). The CaP and CPS groups were weak in the generation of ALP. Notably, the ALP production in the CPSB and CPSBA groups had a large increase after a 14-day culture. With the help of BBR, the CPSB and CPSBA groups demonstrated durable and high activity of ALP in the first and second weeks. ALP is recognized as the early osteogenic marker. Limited by the strong adsorption properties of porous CaP scaffold, the staining tests were hard to promote. In this work, samples with the addition of BBR present a satisfying osteoinductivity, which is consistent with the findings of the previous studies [15,33,34].

The CPS, CPSB, and CPSBA samples have built a third-level SF coating on the bare CaP samples. Although this kind of modification has established a more biomimetic structure compared with CaP scaffolds, the superficial area and roughness have been reduced in a way. The initial attachment never represents the real condition of cell proliferation. The 5-day CCK-8 data showed no significant difference among the groups. Therefore, it is believed that SF coating has really induced cell growth after adhesion. Thus, this kind of layer-by-layer fabrication promotes cell proliferation despite reducing initial adhesion.

Integrins are the main receptors on the surface of cells that combine to ECM [35,36]. When cells are exposed to material, the integrins would search for the specific binding site, such as RGD peptides (Arg-Gly-Asp), to adhere on the material surface [37]. Once the integrins are bound to RGD peptides, regulation signals will be activated and transduced into cells, eventually leading to cytoskeleton remodeling and cells directional stretching [38]. The final termination of the work is to fabricate the structure and composition of biomaterials to mimic natural bone tissue. The SF coating was designed to mimic ECM, but SF lacks RGD sequence. Thus, the CPS, CPSB, CPSBA samples showed relatively slow initial adhesion. The addition of BBR helped to overcome the shortcomings and enhanced the cell spreading, which is similar to the results of the previous study [15,34].

4 Conclusions

This research investigated BBR/nAg/SF biomimetic CaP scaffolds for enhancing osteogenesis and antibacterial functions. The fabrication, characterization analysis, *in vitro* biocompatibility, and antibacterial functions were studied. The results indicated that the porous CaP ceramic with micron pores ranged from 250 to 600 μm in size, which were obtained by gas foaming method to mimic the natural bone structures. The second-level spongy-like structure with abundant capillary pores ranged from 500 nm to 10 μm was formed during the sintering period. The third-level structure was achieved by filling BBR, nAg, and fibroin gel liquid into the above porous structures. The cytocompatibility, antimicrobial activity, and osteogenic potential were evaluated *in vitro*, and the results indicated that this scaffold could significantly promote the antibacterial effects. At the same time, such scaffold showed improved osteogenic functions. For further study, the mechanism behind the antimicrobial and osteoinductive function of BBR/nAg coating will be explored. This new biomimetic CaP scaffold with functions of antibacterial and osteogenesis properties is a promising candidate for bone tissue regeneration.

Abbreviations

ALP	alkaline phosphatase
BBR	berberine
CaP	calcium phosphate
ECM	extracellular matrix

EDS	energy-dispersive X-ray spectroscopy
LB	Luria–Bertani
MRSA	methicillin-resistant *S. aureus*
nAg	Ag nanoparticles
PDA	polydopamine
PSMs	phenol-soluble modulins
SF	silk fibroin
TCM	traditional Chinese medicine

Acknowledgments: This work was supported by the National Key Research and Development Program of China (No. 2018YFC1106800 and 2018YSF1105600), the National Natural Science Foundation of China (31971251), the Sichuan Province Science & Technology Department Projects (2016CZYD0004, 2017SZ0001, 2018GZ0142, 2019YFH0079, and 2019JDTD0008), the Research Foundation for Young Teachers of Sichuan University (2018SCUH0017), and the "111" Project (No. B16033).

Author contributions: Cheng Hu, Lina Wu, and Xiujuan Xu fabricated the materials. Huan Sun, Peng Gao, and Chenxi Zhang studied *in vitro* cell culturing. Yujiang Fan and Jie Liang analyzed the microstructure and antibacterial properties. Changchun Zhou and Jianxun Sun proposed the experimental design and conducted the osteoinductivity test. Xuedong Zhou and Xingdong Zhang supervised the work.

Conflict of interest: The authors declare that there is no conflict of interest regarding the publication of this paper.

References

[1] Zhang B, Pei X, Zhou C, Fan Y, Jiang Q, Ronca A, et al. The biomimetic design and 3D printing of customized mechanical properties porous Ti6Al4V scaffold for load-bearing bone reconstruction. Mater Des. 2018;152(15):30–9.

[2] Zhang B, Sun H, Wu L, Ma L, Xing F, Kong Q, et al. 3D printing of calcium phosphate bioceramic with tailored biodegradation rate for skull bone tissue reconstruction. Bio-Des Manufact. 2019;2:161–71.

[3] Dong Z, Ni Y, Yang X, Hu C, Sun J, Li L, et al. Characterization and analysis of fluoride calcium silicate composite interface in remineralization of dental enamel. Composites Part B. 2018;153:393–7.

[4] Pei X, Ma L, Zhang B, Sun J, Sun Y, Fan Y, et al. Creating hierarchical porosity hydroxyapatite scaffolds with osteoinduction by three-dimensional printing and microwave sintering. Biofabrication. 2017;9:45008.

[5] Zhou P, Xia Y, Cheng X, Wang P, Xie Y, Xu S. Enhanced bone tissue regeneration by antibacterial and osteoinductive silica-Hacc-Zein composite scaffolds loaded with Rhbmp-2. Biomaterials. 2014;35:10033–45.

[6] Brown ED, Wright GD. Antibacterial drug discovery in the resistance era. Nature. 2016;529:336–343.

[7] Chen Y, Sun W, Qu D, Ma Y, Liu C, Zhou J. Enhanced stability and antibacterial efficacy of a traditional chinese medicine-mediated silver nanoparticle delivery system. Int J Nanomed. 2014;9:5491–502.

[8] Zhu L, Zhao L, Wang H, Wang Y, Pan D, Yao J, et al. Oroxylin a reverses p-glycoprotein-mediated multidrug resistance of Mcf7/Adr cells by G2/M arrest. Toxicol Lett. 2013;219:107–15.

[9] Wojtyczka R, Dziedzic A, Kępa M, Kubina R, Kabała-Dzik A, Mularz T, et al. Berberine enhances the antibacterial activity of selected antibiotics against coagulase-negative Staphylococcus strains *in vitro*. Molecules. 2014;19:6583–96.

[10] Kuo C, Chi C, Liu T. The anti-inflammatory potential of berberine *in vitro* and *in vivo*. Cancer Lett. 2004;203:127–137.

[11] Bandyopadhyay S, Patra PH, Mahanti A, Mondal DK, Dandapat P, Bandyopadhyay S, et al. Potential antibacterial activity of berberine against multi drug resistant enterovirulent *Escherichia coli* isolated from yaks (Poephagus Grunniens) with haemorrhagic diarrhoea. Asian Pac J Trop Med. 2013;6:315–9.

[12] Zuo G, Li Y, Han J, Wang G, Zhang Y, Bian Z. Antibacterial and synergy of berberines with antibacterial agents against clinical multi-drug resistant isolates of methicillin-resistant *Staphylococcus aureus* (Mrsa). Molecules. 2012;17:10322–30.

[13] Chu M, Zhang M, Liu Y, Kang J, Chu Z, Yin K, et al. Role of berberine in the treatment of methicillin-resistant *Staphylococcus aureus* infections. Sci Rep. 2016;6:24748.

[14] Dziedzic A, Wojtyczka R, Kubina R. Inhibition of oral streptococci growth induced by the complementary action of berberine chloride and antibacterial compounds. Molecules. 2015;20:13705–24.

[15] Tao K, Xiao D, Weng J, Xiong A, Kang B, Zeng H. Berberine promotes bone marrow-derived mesenchymal stem cells osteogenic differentiation via canonical Wnt/B-catenin signaling pathway. Toxicol Lett. 2016;240:68–80.

[16] Doty RC, Tshikhudo TR, Brust M, Fernig DG. Extremely stable water-soluble Ag nanoparticles. Chem Mater. 2005;17:4630–5.

[17] Le AT, LeTT, Tam PD, Huy PT, Huy TQ, Van Hieu N, et al. Synthesis of oleic acid-stabilized silver nanoparticles and analysis of their antibacterial activity. Mater Sci Eng C. 2010;30:910–6.

[18] Lee S, Shin S, Lee S, Seo J, Lee T. Ag nanowire reinforced highly stretchable conductive fibers for wearable electronics. Adv Funct Mater. 2015;25:3114–21.

[19] Lok CN, Ho C, Chen R, He Q, Yu W, Sun H, et al. Silver Nanoparticles: partial oxidation and antibacterial activities. JBIC J Biol Inorg Chem. 2007;12:527–534.

[20] Sable SV, Kawade S, Ranade S, Joshi S. Bioreduction mechanism of silver nanoparticles. Mater Sci Eng C. 2020;107:110299.

[21] Qi Y, Ye J, Ren S, Lv J, Zhang S, Che Y, et al. *In situ* synthesis of metal nanoparticles@metal–organic frameworks: highly effective catalytic performance and synergistic antimicrobial activity. J Hazard Mater. 2020;387:121687.

[22] Arakha M, Borah SM, Saleem M, Jha AN, Jha S. Interfacial assembly at silver nanoparticle enhances the antibacterial efficacy of Nisin. Free Radic Biol Med. 2016;101:434–45.

[23] Singh YP, Bhardwaj N, Mandal BB. Potential of agarose/silk fibroin blended hydrogel for *in vitro* cartilage tissue engineering. ACS Appl Mater Interfaces. 2016;8:21236–49.
[24] Melke J, Midha S, Ghosh S, Ito K, Hofmann S. Silk fibroin as biomaterial for bone tissue engineering. Acta Biomater. 2016;31:1–16.
[25] Thai TH, Nuntanaranont T, Kamolmatyakul S, Meesane J. *In vivo* evaluation of modified silk fibroin scaffolds with a mimicked microenvironment of fibronectin/decellularized pulp tissue for maxillofacial surgery. Biomed Mater. 2018;13:15009.
[26] Fei X, Jia M, Du X, Yang Y, Zhang R, Shao Z, et al. Green synthesis of silk fibroin-silver nanoparticle composites with effective antibacterial and biofilm-disrupting properties. Biomacromolecules. 2013;14:4483–8.
[27] Su D, Yao M, Liu J, Zhong Y, Chen X, Shao Z. Enhancing mechanical properties of silk fibroin hydrogel through restricting the growth of B-sheet domains. ACS Appl Mater Interfaces. 2017;9:17489–98.
[28] Pan Y, Xiong D. Study on compressive mechanical properties of nanohydroxyapatite reinforced poly(vinyl alcohol) gel composites as biomaterial. J Mater Sci Mater Med. 2009;20:1291–7.
[29] Huang J, Pang L, Chen Z, Tan X. Dual-delivery of vancomycin and icariin from an injectable calcium phosphate cement-release system for controlling infection and improving bone healing. Mol Med Rep. 2013;8:1221–7.
[30] Lai Y, Cao H, Wang X, Chen S, Zhang M, Wang N, et al. Porous composite scaffold incorporating osteogenic phytomolecule icariin for promoting skeletal regeneration in challenging osteonecrotic bone in rabbits. Biomaterials. 2018;153:1–13.
[31] Xue L, Jiao L, Wang Y, Nie Y, Han T, Jiang Y, et al. Effects and interaction of icariin, curculigoside, and berberine in Er-Xian decoction, a traditional chinese medicinal formula, on osteoclastic bone resorption. Evidence-Based Complementary and Alternative Medicine. 2012;2012:490843.
[32] Sun H, Hu C, Zhou C, Wu L, Sun J, Zhou X, et al. 3D printing of calcium phosphate scaffolds with controlled release of antibacterial functions for jaw bone repair. Mater Des. 2020;189:108540.
[33] Lee HW, Suh JH, Kim H, Kim AY, Park SY, Shin CS, et al. Berberine promotes osteoblast differentiation by Runx2 activation with P38 Mapk. J Bone Miner Res. 2008;23:1227–1237.
[34] Liu J, Zhao X, Pei D, Sun G, Li Y, Zhu C, et al. The promotion function of berberine for osteogenic differentiation of human periodontal ligament stem cells via Erk-Fos pathway mediated by Egfr. Sci Rep. 2018;8:2848.
[35] Sun Z, Guo SS, Fässler R. Integrin-mediated mechanotransduction. J Cell Biol. 2016;215:445–456.
[36] Hamidi H, Ivaska J. Every step of the way: integrins in cancer progression and metastasis. Nat Rev Cancer. 2018;18:1.
[37] Huettner N, Dargaville TR, Forget A. Discovering cell-adhesion peptides in tissue engineering: beyond Rgd. Trends Biotechnol. 2018;36:S1315849351.
[38] Sobers CJ, Wood SE, Mrksich M. A gene expression-based comparison of cell adhesion to extracellular matrix and Rgd-terminated monolayers. Biomaterials. 2015;52:385–94.